Failed CTL/NK cell killing and cytokine hypersecretion are directly linked through prolonged synapse time

Misty R. Jenkins,[1,3] Jesse A. Rudd-Schmidt,[2,3] Jamie A. Lopez,[2,3] Kelly M. Ramsbottom,[1,3] Stuart I. Mannering,[5,6] Daniel M. Andrews,[3] Ilia Voskoboinik,[2,3,4]* and Joseph A. Trapani[1,3]*

[1]Cancer Cell Death and [2]Killer Cell Biology Laboratories, Peter MacCallum Cancer Centre, East Melbourne, Victoria 3002, Australia
[3]The Sir Peter MacCallum Department of Oncology; [4]Department of Genetics; and [5]Department of Medicine, St. Vincent's Hospital; The University of Melbourne, Parkville, Victoria 3010, Australia
[6]Immunology and Diabetes Unit, St. Vincent's Institute of Medical Research, Fitzroy, Victoria 3065, Australia

Failure of cytotoxic T lymphocytes (CTLs) or natural killer (NK) cells to kill target cells by perforin (Prf)/granzyme (Gzm)–induced apoptosis causes severe immune dysregulation. In familial hemophagocytic lymphohistiocytosis, Prf-deficient infants suffer a fatal "cytokine storm" resulting from macrophage overactivation, but the link to failed target cell death is not understood. We show that prolonged target cell survival greatly amplifies the quanta of inflammatory cytokines secreted by CTLs/NK cells and that interferon-γ (IFN-γ) directly invokes the activation and secondary overproduction of proinflammatory IL-6 from naive macrophages. Furthermore, using live cell microscopy to visualize hundreds of synapses formed between wild-type, Prf-null, or GzmA/B-null CTLs/NK cells and their targets in real time, we show that hypersecretion of IL-2, TNF, IFN-γ, and various chemokines is linked to failed disengagement of Prf- or Gzm-deficient lymphocytes from their targets, with mean synapse time increased fivefold, from ∼8 to >40 min. Surprisingly, the signal for detachment arose from the dying target cell and was caspase dependent, as delaying target cell death with various forms of caspase blockade also prevented their disengagement from fully competent CTLs/NK cells and caused cytokine hypersecretion. Our findings provide the cellular mechanism through which failed killing by lymphocytes causes systemic inflammation involving recruitment and activation of myeloid cells.

CORRESPONDENCE
Misty R. Jenkins:
misty.jenkins@petermac.org
OR
Joseph A. Trapani:
joe.trapani@petermac.org

Abbreviations used: CBA, cytokine bead array; FHL, familial hemophagocytic lymphohistiocytosis; Gzm, granzyme; IS, immunological synapse; PI, propidium iodide; Prf, perforin; XIAP, X-linked inhibitor of apoptosis protein.

CTLs and NK cells are essential eliminators of cancerous and virus-infected cells. After immunological synapse (IS) formation, these "killer cells" release perforin (Prf) and granzymes (Gzms) from their specialized secretory vesicles (Jenkins and Griffiths, 2010). Prf transiently forms pores on the target cell membrane, enabling diffusion of proapoptotic serine protease Gzms into the cytosol (Lopez et al., 2013a,b), to trigger caspase activation via both the extrinsic and intrinsic (mitochondrial) pathways. In our recent study, target cell death was thus initiated within 2–3 min of Prf pore formation (Lopez et al., 2013a). After detaching, a CTL/NK cell can rapidly attack other target cells, and "serial killing" of up to 10 cells can be observed for NK cells in vitro within 6 h (Choi and Mitchison, 2013).

Prf-dependent cytotoxicity is critical for human immune homeostasis: infants with biallelic *PRF1* gene mutations develop a fatal immune dysregulation syndrome, type 2 familial hemophagocytic lymphohistiocytosis (FHL2; Stepp et al., 1999). This hyperinflammatory state reflects release of the proinflammatory cytokine IFN-γ by CTLs/NK cells after their failure to shut down the antigen-driven phase of the immune response and copious IL-1β, IL-6, and TNF that then emanate from the myeloid compartment. Intractable fever, pancytopenia,

*I. Voskoboinik and J.A. Trapani contributed equally to this paper.

The Rockefeller University Press $30.00
J. Exp. Med. 2015 Vol. 212 No. 3 307–317
www.jem.org/cgi/doi/10.1084/jem.20140964

The Journal of Experimental Medicine

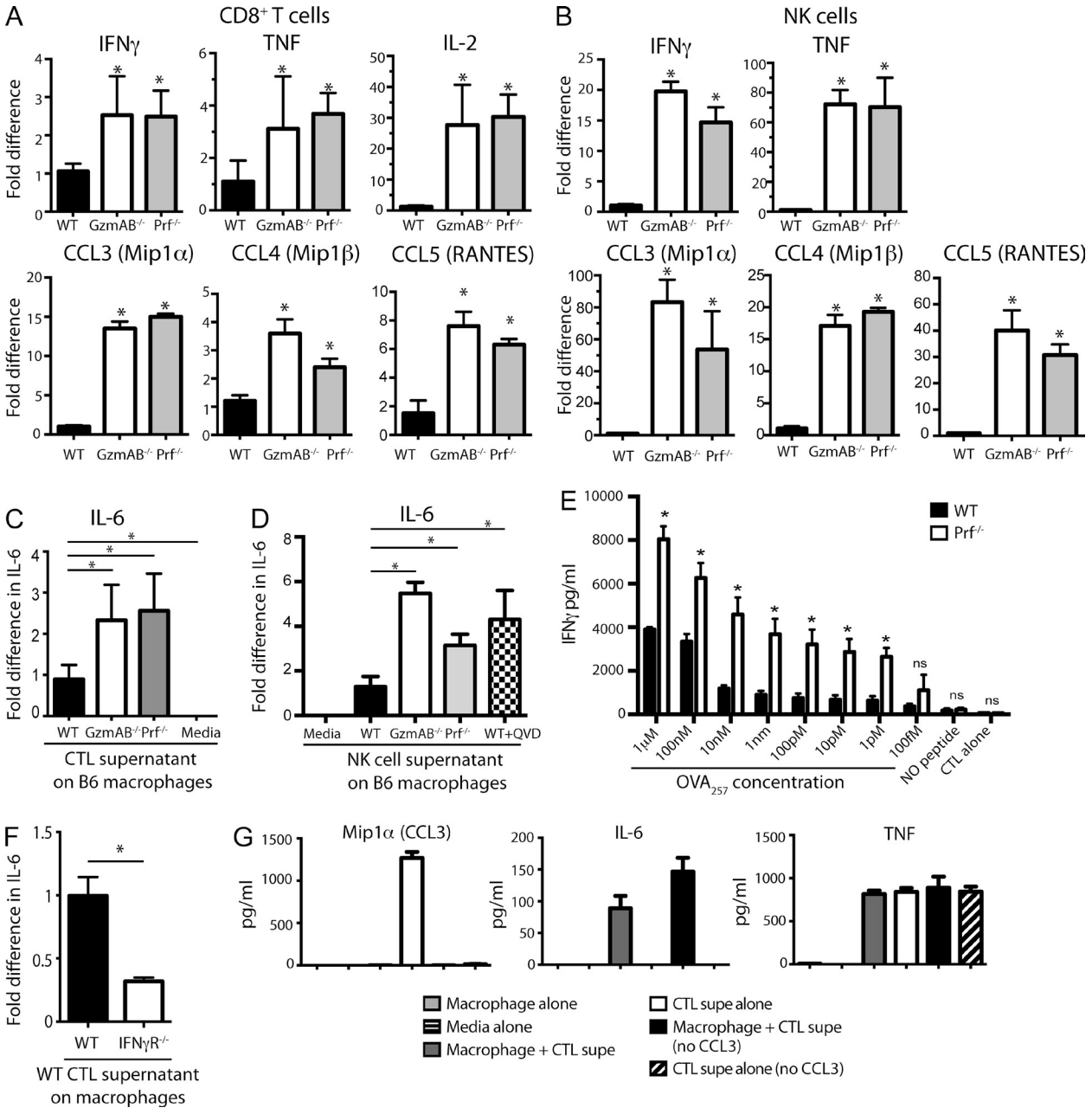

Figure 1. CTLs and NK cells lacking Prf and GzmAB overproduce cytokines, which induces myeloid cells to produce IL-6. (A and B) CTLs (OTI, OTI.GzmAB$^{-/-}$, or OTI.Prf$^{-/-}$) were added to MC57-OVA$_{257}$ target cells (A), or NK cells lacking GzmAB or Prf were added to MC57 target cells (B), and supernatant was collected after 5 h. Supernatants were analyzed for IFN-γ, TNF, IL-2, CCL3, CCL4, and CCL5 by CBA. Shown is the fold difference above WT (mean ± SD) of four independent experiments. (C and D) Each corresponding CTL target or NK target cell supernatant was cultured with bone marrow–derived syngeneic macrophages (generated in vitro for 5 d with M-CSF), and IL-6 production was analyzed after 48 h by CBA. Shown is the fold difference pooled from three experiments for CTLs (mean ± SEM; C) or one representative experiment of two for NK cells (mean ± SD; D). (E) CTLs produce cytokines in an antigen-dependent manner. The experiment in A was repeated but using MC57 target cells pulsed with titrated peptide. Supernatants were analyzed for concentration of IFN-γ produced (mean ± SD) of three independent pooled experiments. Statistical significance compares OTI with OTI.Prf$^{-/-}$ within individual peptide concentration. (F) The CTL target supernatants (from A) were also co-cultured with B6.*IFNγR*$^{-/-}$ macrophages, and IL-6 production was measured by CBA after 48 h. Shown are triplicates of a representative experiment of two (mean ± SD). Statistical significance was determined by Tukey's post-hoc ANOVA. (G) Immunodepletion of CCL3 and CBA. CTL target cell supernatant (from A) was depleted of CCL3 by immunoprecipitation with anti-CCL3 antibody and protein A. The remaining cytokine cocktail was co-cultured with syngeneic macrophages for 48 h. Shown are the concentrations of CCL3, IL-6, and TNF (control) detected in the macrophage culture, as detected by CBA (mean ± SEM of two independent pooled experiments). *, $P < 0.05$.

multiorgan failure, and death result unless patients receive cytotoxic agents or, ultimately, bone marrow transplantation (Janka, 2012). *Prf1* knockout mice also develop a fatal FHL-like state after challenge with certain antigenic or viral stimuli (Kägi et al., 1994; Jordan et al., 2004; van Dommelen et al., 2006). In other congenital forms of FHL, *PRF1* expression is normal, but the trafficking, docking, or exocytosis of cytotoxic granules is impaired and Prf is not delivered to the IS (Sieni et al., 2014). Linking failed killing by lymphoid cells with fatal hyperinflammation, mediated principally by myeloid cells (particularly macrophages), remains a central unanswered question.

In the current study, we discovered that failure of Prf/Gzm cytotoxicity by human or mouse CTLs/NK cells dramatically extends the life of the IS, leading to repetitive calcium signaling and their pronounced hypersecretion of inflammatory cytokines and chemokines. In turn, this inflammatory "cocktail" was capable of activating naive macrophages and evoking IL-6 secretion. By blocking caspase processing in the target cell, we further demonstrated that disengagement of CTLs/NK cells from the target was specifically dependent on target cell death, revealing that the dying cell provides a caspase-dependent signal for detachment. Our study provides a mechanistic explanation for the immunopathology of FHL and links fatal myeloid cell activation with marked delay or failure of target cell death mediated by lymphocytes. Furthermore, our finding that corruption of apoptotic pathways in tumor target cells attacked by CTLs/NK cells can influence the resultant inflammatory milieu has implications for our understanding of the immune response to cancer and the mode of action of immune-based therapies that aim to augment lymphocytotoxicity.

RESULTS AND DISCUSSION

Infants with defects in lymphocytotoxicity, especially those that completely lack functional Prf (FHL2), frequently undergo a fatal cytokine storm soon after birth, with elevated circulating IFN-γ, TNF, and IL-6 (Stepp et al., 1999; Janka, 2012). To further our understanding of this fatal condition and its link to myeloid cell activation, we explored a possible link between failed Prf-dependent cell death and cytokine hypersecretion by both lymphocytes and macrophages.

Failure to kill target cells enhances cytokine secretion by CTLs/NK cells

We first generated antigen-restricted CTLs from transgenic C57BL/6.OTI (OTI) mice (Strasser et al., 1990a; Hogquist et al., 1994) or from syngeneic mice that lacked Prf (OTI.Prf$^{-/-}$) or both GzmA and GzmB, the two most potently cytotoxic Gzms (OTI.GzmAB$^{-/-}$; Strasser et al., 1990b; Jenkins et al., 2007, 2008; Susanto et al., 2013). We coincubated OTI, OTI.Prf$^{-/-}$, or OTI.GzmAB$^{-/-}$ CTLs with OVA_{257}-pulsed MC57 target cells and measured cytokine release into the supernatant. Incubation for 5 h produced robust target cell killing by OTI CTLs, but almost none in the absence of Prf or GzmAB, despite the T cells having undergone similar activation and proliferation in vitro (Fig. S1, A and B; Hoves et al., 2011).

We found a significant increase in cytokine release by CTLs lacking either Prf or GzmAB compared with WT CTLs, including IFN-γ (>2-fold), TNF (>3-fold), and IL-2 (25–30-fold; Fig. 1 A). Secretion of the chemokines CCL3 (Mip1α; 13–15-fold), CCL4 (Mip1β; ∼2.5–3.5-fold), and CCL5 (RANTES; ∼6–7-fold) was also markedly increased (Fig. 1 A); however, IL-1α, IL-1β, and IL-6 were not detected. As overall CTL/target cell avidity influences cytokine responses (La Gruta et al., 2006), the concentration of OVA_{257} peptide was varied, and cytokine secretion was again estimated. As expected, IFN-γ secretion was related to peptide concentration; however, OTI.Prf$^{-/-}$ CTLs released more IFN-γ at every peptide concentration (Fig. 1 E).

Given that the symptoms and signs of FHL2 can occur within a few weeks of birth and neonates have relatively poor CD8$^+$ T cell effector responses, we also examined the cytokine response of primary NK cells devoid of Prf or GzmAB. Prf- or GzmAB-deficient mouse NK cells produced similar results as CTLs; indeed, the fold increase in cytokine secretion was greater than that for an equivalent number of clonotypic CTLs, varying from 15–20-fold for IFN-γ and CCL4 to 30–80-fold for TNF, CCL3, and CCL5 (Fig. 1 B). Both TNF and CCL3 play a key role in pancytopenia (Janka, 2012) but have been thought to originate from macrophages. However, our data suggest that NK cells may also prove to be an additional source of the cytokine storm in FHL2 patients, particularly at the early stage of the disease.

Macrophage-derived IL-6 is consistently elevated in the serum of FHL patients and reflects active disease (Janka, 2012). We demonstrated that the CTL/target cell supernatants induced naive syngeneic macrophages to secrete proinflammatory IL-6 with coincubation (Fig. 1 C). OTI.Prf$^{-/-}$ supernatants induced ∼2.5-fold higher production of IL-6 over 24 h compared with OTI CTL/target cell cultures (Fig. 1 C). The same supernatants also strongly induced MHC class I expression and other markers indicative of macrophage activation (Fig. S2). Consistent with the increased levels of cytokines elaborated by NK cells compared with CTLs, more macrophage IL-6 was secreted in response to the cytokine cocktail produced by Prf$^{-/-}$ or GzmAB$^{-/-}$ NK cells, typically three- to sixfold (Fig. 1 D). The release of IL-6 was largely (∼75%) inhibited when we used syngeneic macrophages lacking the receptor for IFN-γ (Fig. 1 F), indicating a pivotal role for this cytokine in IL-6 induction and consistent with earlier studies (Jordan et al., 2004; Pachlopnik Schmid et al., 2009). In contrast, a neutralizing mAb to CCL3 had no effect on the release of IL-6 (Fig. 1 G).

Failure of target cell death results in a sustained IS and repetitive calcium signaling

The markedly aberrant cytokine secretion by Prf$^{-/-}$ and GzmAB$^{-/-}$ cytotoxic lymphocytes prompted us to closely examine the interaction of killer cells with target cells in real time. We used time-lapse microscopy methodologies that

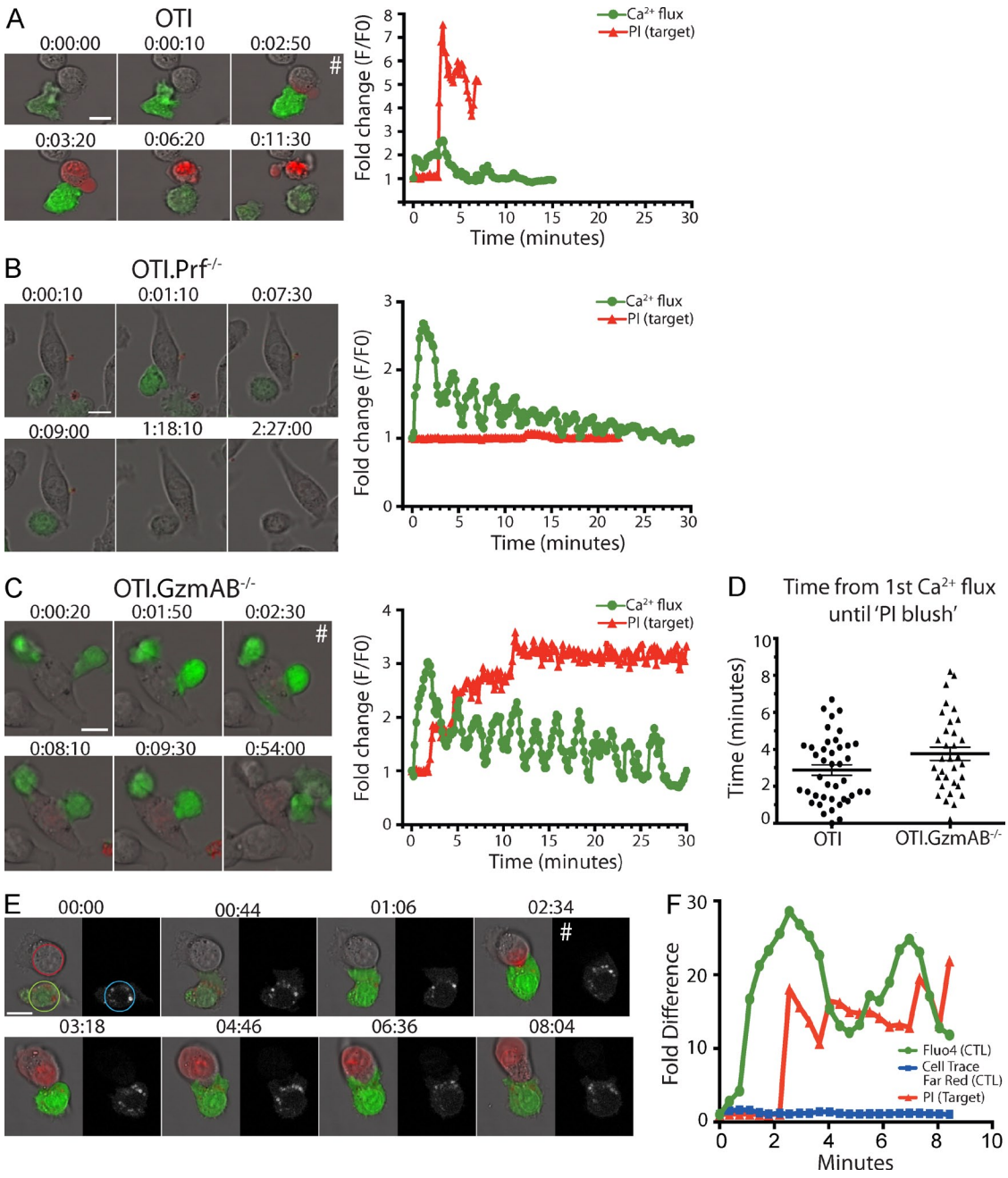

Figure 2. Live cell imaging of CTL with targets. (A–C) Time-lapse microscopy of fluo-4–AM-labeled OTI, OTI.Prf$^{-/-}$, and OTI.GzmAB$^{-/-}$ CTLs killing MC57 target cells in the presence of 100 µM PI. OTI (A), OTI.Prf$^{-/-}$ (B), or OTI.GzmAB$^{-/-}$ (C) with MC57-OVA$_{257}$ target cells are shown. Images were acquired every 10 s and show fluo-4 (green)/PI (red)/brightfield overlay. Images depict conjugation of the CTL with the target cell and sequential elevations in CTL intracellular Ca^{2+}, followed by cytosolic diffusion of PI into the target cell (A and C). Images are representative of 53, 26, and 26 conjugates, respectively. See also Videos 1–3. Graphs beside each montage display the fold change (F/F_0) of the fluo-4 fluorescence over time in the CTL and fold change in PI fluorescence by the target cells. (D) The time from first calcium flux until PI blush into target cell for targets "hit" by OTI or OTI.GzmAB$^{-/-}$. Data represent mean ± SD of 41 and 33 conjugates, respectively. Student's *t* test showed no statistical difference. (E) Representative live cell imaging of CTLs with targets with internal fluorescence control. The identical experiment to A was performed, with CTLs also labeled with cell trace far-red. Images were acquired every 22 s, and shown is a montage of fluo-4 (green)/PI (red)/brightfield overlay (left panels) and cell trace far-red (corresponding right panels). Images depict conjugation of the CTLs with the target cell and sequential elevations in CTL intracellular Ca^{2+} (green), followed by cytosolic diffusion of PI into the target cell (red). Time above the montage shows minutes:seconds. The first panel shows regions in which fluorescence intensity was measured. See also Video 4. (F) Graph of montage displaying the fold change (F/F_0) of the fluo-4 (red) and cell trace violet (blue) fluorescence over time in the CTL and fold change in PI fluorescence in the target cell. # denotes PI blush. Bars, 10 µm.

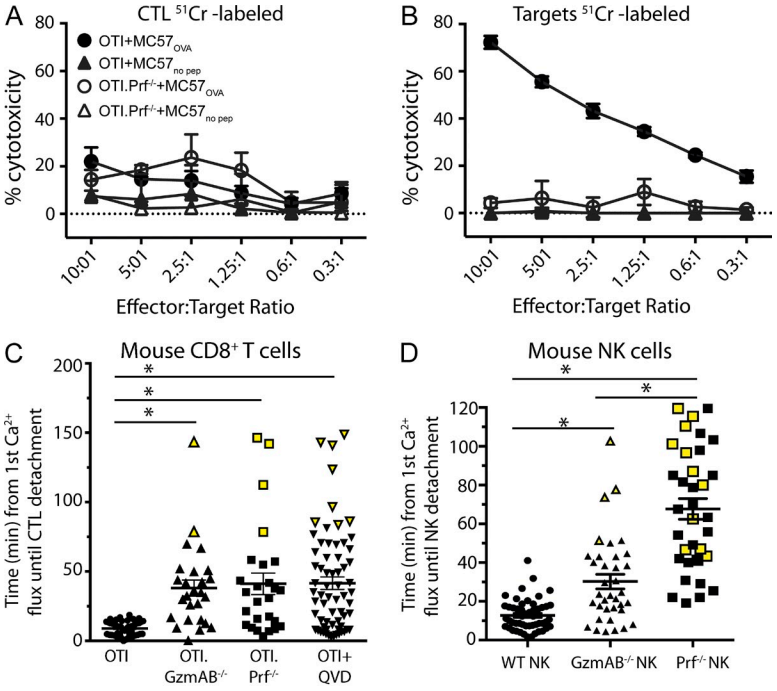

Figure 3. ^{51}Cr-labeled OTI CTLs demonstrate survival of the killer cell, and target cell death is required for rapid detachment of the killer cell. (A and B) OTI (closed) or OTI.Prf$^{-/-}$ (open) CTLs were incubated for 5 h with MC57 target cells pulsed with 1 µM OVA_{257} peptide (or with no peptide as a control). Either the CTLs (A) or MC57 cells (B) were labeled with ^{51}Cr to determine ^{51}Cr release. Shown is the percentage of specific ^{51}Cr release as the mean ± SD of two independent pooled experiments. (C) Time from calcium flux to killer cell detachment from target cells. OTI, OTI.GzmAB$^{-/-}$, or OTI.Prf$^{-/-}$ CTLs labeled with fluo-4–AM were added to MC57-OVA_{257} target cells in the absence or presence of caspase inhibitor QVD. After conjugate formation, time was measured from first Ca^{2+} flux in CTL until its detachment from the target. Each data point represents one conjugate, and means are 8.5 ± 0.7, 38.1 ± 5.7, 41.2 ± 7.7, and 41.6 ± 4.4 min (SEM; n = 53, 26, 26, and 66, respectively). (D) Mouse NK cells (WT B6 or GzmAB$^{-/-}$ or Prf$^{-/-}$) were labeled with fluo-4–AM and added to MC57 target cells. Shown is the time from first calcium flux until detachment from the target: 12.77 ± 1.1, 30.2 ± 3.7, and 67.66 ± 5.3 min (SEM; n = 51, 36, and 34, respectively), where each point represents a single NK cell–target cell conjugate. All data points shown in yellow indicate CTL–target cell conjugates that were still attached at the end of the video and therefore underestimate the duration of attachment. Statistical significance was determined by Tukey's post-hoc ANOVA. *, $P < 0.05$.

precisely pinpoint the instant that Prf permeabilizes the target cell plasma membrane within the IS (Lopez et al., 2013a,b). Calcium influx into the OTI CTLs labeled with the calcium fluorophore fluo-4–AM indicated the formation of a bona fide IS with an OVA_{257} peptide–pulsed MC57 target cell and the stimulus for degranulation (Fig. 2 A). The formation of Prf pores on the target cell was inferred from the rapid diffusion of propidium iodide (PI) into the target cell, producing a sudden strong "blush" in red fluorescence (Fig. 2 A and Video 1), consistent with our earlier studies (Lopez et al., 2013a,b). Target cell rounding, an early hallmark of apoptosis, soon followed, and the CTLs then detached from the target cell (see below). In contrast, although OTI.Prf$^{-/-}$ CTLs engaged their targets (as confirmed by Ca^{2+} influx), they failed to elicit a PI blush in the target cell because of the absence of Prf (Fig. 2 B and Video 2). Strikingly, although a Ca^{2+} flux of similar amplitude occurred in the two types of CTLs, green fluorescence (Ca^{2+} flux) continued to oscillate every 2–3 min in Prf$^{-/-}$ CTLs, and they remained conjugated with the target cell for protracted periods of time (Fig. 2 B and Video 2).

In comparison with OTI.Prf$^{-/-}$ CTLs, OTI.GzmAB$^{-/-}$ cells offered the opportunity to study CTL–target cell conjugates, in which apoptosis was delayed because of a lack of Gzms. Despite delivering Prf and thus enabling us to define the precise moment of pore formation by uptake of PI (Fig. 2 C and Video 3), these cells induced little target cell death over 5 h (Fig. S1 A). In the absence of the early morphological changes of apoptosis seen with WT CTLs (cell rounding and intense membrane blebbing), cytosolic calcium levels oscillated in the OTI.GzmAB$^{-/-}$ CTLs, and their detachment from target cells was greatly delayed, similar to the Prf$^{-/-}$ CTLs (Fig. 2 C and below). The concordance of our data with Prf- or GzmAB-null CTLs indicated that pore formation on the target cell per se was insufficient to trigger target cell detachment. Rather, death of the target cell appeared to be required (see below).

As cell movement and changes in their morphology might incidentally affect pixel fluorescence intensity, in some experiments we colabeled OTI CTLs with fluo-4–AM (green) and ion-neutral cell trace dye (far-red) as an internal reference. The far-red signal did not oscillate, excluding this possible source of artifact (Fig. 2, E and F; and Video 4). We also confirmed (Lopez et al., 2013a) OTI T cell survival by the lack of PI uptake (<1% of all ISs) and also the lack of ^{51}Cr release when CTLs rather than the target MC57 cells were labeled with ^{51}Cr (Fig. 3, A and B).

Failed target cell death greatly delays detachment of the killer cell

Next, we compared the longevity of individual ISs, i.e., the time from the first Ca^{2+} flux into a given CTL until it detached from its target cell. Remarkably, although OTI CTLs maintained the IS for 7.6 ± 1.1 min, detachment was significantly delayed approximately fivefold for the OTI.Prf$^{-/-}$ or OTI.GzmAB$^{-/-}$ CTLs (38 ± 8 min and 41 ± 6 min, respectively; Fig. 3 C). In contrast, the time lapsed between the calcium signaling in the killer cell and PI influx into the target was not significantly different for OTI and OTI.GzmAB$^{-/-}$ CTLs (3.7 ± 0.4 min vs. 2.9 ± 0.3 min), indicating that TCR signaling, degranulation, and Prf pore formation were not altered between the two cell types (Fig. 2 D). This result

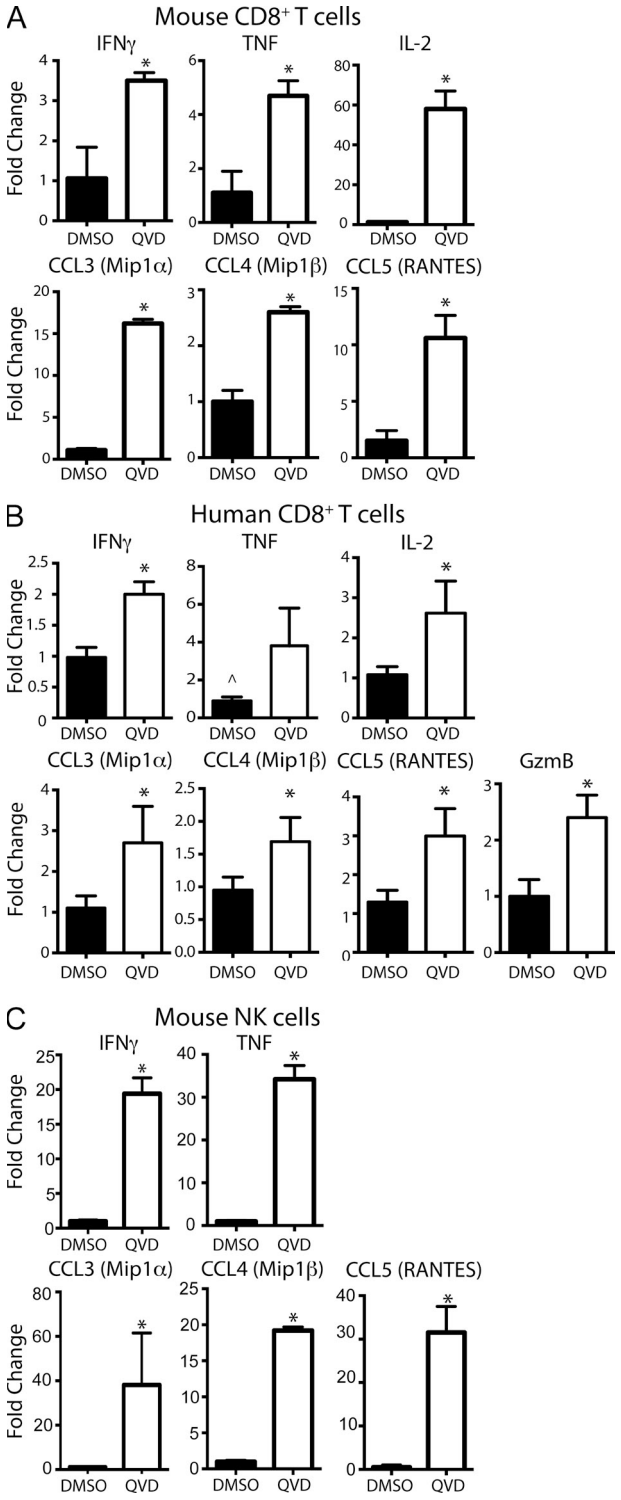

Figure 4. Overproduction of cytokines in the absence of target cell death. (A–C) CBA of cytotoxic lymphocyte target cell supernatants (as in Fig. 1) in the presence or absence of QVD to block target cell death. Graphs show mouse CTL (A), human CTL (B), and mouse NK cell (C) fold change of cytokine/chemokines, and data represent mean ± SEM of three independent experiments. Statistical significance was determined by Tukey's post-hoc ANOVA. *, $P < 0.05$; ^, $P = 0.06$.

confirmed that the various CTL populations were equally activated with respect to degranulation (Hoves et al., 2011) and the absence of Gzms did not impair degranulation or Prf pore formation. Prf- and Gzm-deficient mouse NK cells also remained in synapse with their targets for significantly longer than WT cells (Fig. 3 B). Similar to CTLs, both WT NK cells and GzmAB$^{-/-}$ NK cells displayed a single Ca^{2+} flux before delivery of Prf into the IS (not depicted). Synapse dwell time for NK cells lacking GzmAB was prolonged ~2.5-fold from 12.7 ± 1.1 min to 30.2 ± 3.7 min ($P < 0.0001$) and was even longer in the absence of Prf (~5-fold increase to 67.7 ± 5.3 min; Fig. 3 D). Interestingly, Prf$^{-/-}$ NK cells remained in synapse with their targets for considerably longer than GzmAB$^{-/-}$ NK cells (Fig. 3 D), whereas the corresponding CTLs showed no difference (Fig. 3 C). Despite this, Prf$^{-/-}$ and GzmAB$^{-/-}$ NK cells secreted similar amounts of cytokines after encountering target cells (Fig. 1 B), limiting the significance of this observation for any potential inflammatory sequelae.

In most instances, the Prf$^{-/-}$ or GzmAB$^{-/-}$ killer cells did eventually dissociate from their targets (Fig. 3, C and D), and a proportion were able to detach with similar kinetics as WT killer cells despite failing to induce cell death. Although our data indicate that target cell death is a critical determinant of synapse breakage, we conclude that other mechanisms must also contribute. Although speculative, it is possible that the continual recycling of adhesion molecules to the cell surface and/or the stochastic shearing forces continually applied to the IS because of fluctuations of cell shape may contribute. We propose that in vivo, where functionally impaired CTLs/NK cells have the opportunity to interact with their targets for days or even weeks (rather than 5 h, as in our experiments), more pronounced macrophage and cytotoxic lymphocyte hyperactivation may occur. How Prf-mediated apoptosis down-regulates the immune response is debated, but one proposal is that CTLs are essential for removing "professional" APCs, particularly dendritic cells (Terrell and Jordan, 2013). We support this notion, but our findings show that failure to kill "generic" target cells at an earlier phase of the immune response also induces potent proinflammatory cytokine/chemokine responses, particularly from NK cells.

The signal for detachment arises in the dying target cell and is caspase dependent

The absence of either Prf or GzmAB dramatically increased synapse dwell time, raising the possibility that target cell death per se might provide the key signal for cell detachment, rather than degranulation or the actions of specific cytotoxic molecules. To test this proposition, we presented OVA_{257}-pulsed MC57 target cells to WT OTI CTLs, but delayed apoptosis by preincubating the target cells with Q-VD-OPh (QVD), a broad spectrum caspase inhibitor (Caserta et al., 2003). The CTLs initiated synapses with normal kinetics, but live cell imaging again demonstrated a striking delay in target cell detachment (41.6 ± 4.4 min), similar to that seen in the absence of Prf or GzmAB (Fig. 3 C). This observation confirmed that

the signal for synapse breakage is generated in a caspase-dependent fashion in the target cell and is not intrinsically dependent on the secretion of Prf or Gzms.

We also measured the cytokines secreted by WT OTI CTL upon encountering peptide-labeled target cells in which caspases were blocked with QVD. This resulted in similar increases in IFN-γ, TNF, IL-2, CCL3, CCL4, and CCL5, as we observed with OTI.Prf$^{-/-}$ or OTI.GzmAB$^{-/-}$ CTLs (Fig. 4 A). This observation held across species, as two independent human CTL clones detecting influenza matrix peptide demonstrated very similar delays in breakage of the IS (Fig. 5 and Videos 5 and 6) and elaboration of cytokines (Fig. 4 B). The secretion of GzmB into the culture supernatant was also increased (Fig. 4 B), confirming that the CTLs continued to degranulate when in synapse with an apoptosis-resistant target cell. Cytokine secretion by mouse NK cells incubated with target cells in which caspase activity was blocked was also markedly increased (Fig. 4 C).

QVD powerfully blocks many proapoptotic caspases, including initiator caspases 8/9/10 and effector caspase 3 (Caserta et al., 2003; Kuželová et al., 2011), but it also blocks caspase 12, a polymorphic human caspase with proinflammatory activity (Yeretssian et al., 2009). To confirm that prolonged synapse time and cytokine hypersecretion authentically arose from delayed cell death, we used HeLa target cells that overexpressed B cell lymphoma 2 (Bcl-2), alone or together with X-linked inhibitor of apoptosis protein (XIAP; Waterhouse et al., 2006; Sedelies et al., 2008). Bcl-2 prevents mitochondrial outer membrane permeabilization, thus inhibiting both direct activation of the intrinsic apoptotic pathway in response to BH3-only proteins and amplification of caspase activity through activation of the extrinsic pathway (Strasser et al., 2011). In contrast, XIAP blocks procaspase processing through direct binding (Deveraux and Reed, 1999). Cells overexpressing Bcl-2/XIAP (Fig. 6 A) were exposed to human NK cells (Fig. 6 B), but this only partly reduced ^{51}Cr release. However, when we additionally inhibited GzmB by pretreating the target cells with C20, a specific, cell-permeable human GzmB inhibitor (Willoughby et al., 2002; Sutton et al., 2012), target cell death was reduced by ∼85%. This result supported previous observations from our group that both Bcl-2 overexpression and direct caspase inhibition are required for target cell survival in response to human NK cell attack (Sutton et al., 1997; Sedelies et al., 2008). When we exposed the caspase-inhibited HeLa cells to primary human NK cells as before, the cells remained in synapse for far longer, and the NK cells produced significantly more IFN-γ, TNF, CCL3, CCL4, and CCL5 than controls (Fig. 6 C).

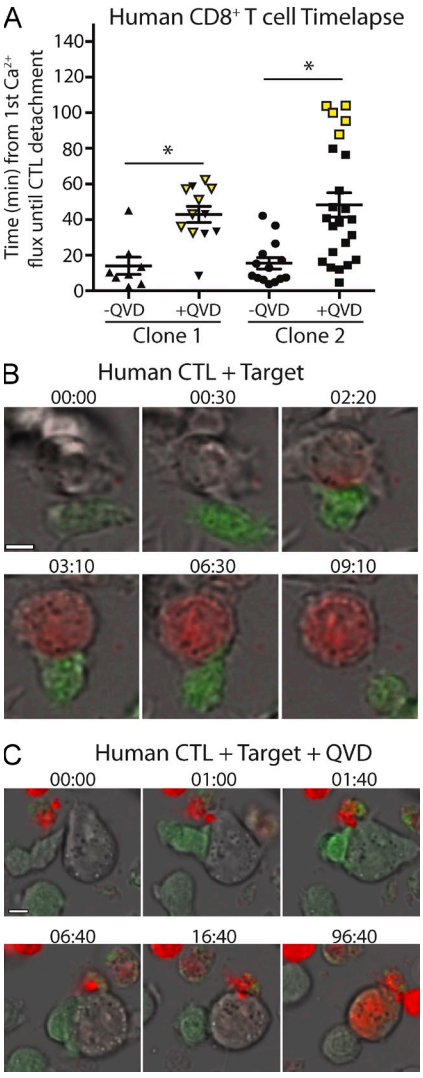

Figure 5. Human CTLs display longer synapse duration in the absence of target cell death. Time-lapse microscopy of fluo-4–AM-labeled human CTLs killing Boleth target cells (prepulsed with GILGFVFTL peptide) in the presence of 100 µM PI ± QVD to block caspases. (A) After conjugate formation, time was measured from the first Ca^{2+} flux in CTL until it detached from the target cell for two human clones. Each point represents a single CTL–target cell conjugate, and all data points in yellow show conjugates that were still attached at the end of the video, therefore underestimating the duration of attachment. The synapse duration was 14 ± 4.8, 42.9 ± 4.4, 15.4 ± 3.2, and 48.2 ± 6.8 min (SEM; n = 8, 12, 14, and 23, respectively). Statistical significance was determined by Tukey's ANOVA. *, $P < 0.05$. Images were acquired every 20 s. (B and C) Montage of human CTLs + Boleth targets (B) and with the addition of QVD (C). Fluo-4 (green)/PI (red)/brightfield overlay is shown. Time corresponds to minutes:seconds. See also Videos 5 and 6. Bars, 5 µm.

Concluding remarks

Overall, our data have important implications for FHL and related inflammatory syndromes (perforinopathies; Voskoboinik and Trapani, 2013). We propose a model where FHL2-related immune pathology is initiated by cross talk of APCs with NK cells at the site of inflammation. In this setting, APCs are activated and produce cytokines. This, in turn, activates NK cells that are embedded in a reciprocal cross talk network with the APCs designed to shape/limit subsequent immune responses (Ferlazzo et al., 2002; Gerosa et al., 2002; Piccioli et al., 2002). In the absence of Prf delivery into the IS, APCs are not eliminated by NK cells and the cycle of activation becomes entrenched and, ultimately, systemic (Ferlazzo, 2012). This systemic cytokine production can enroll CD8$^+$ T cells

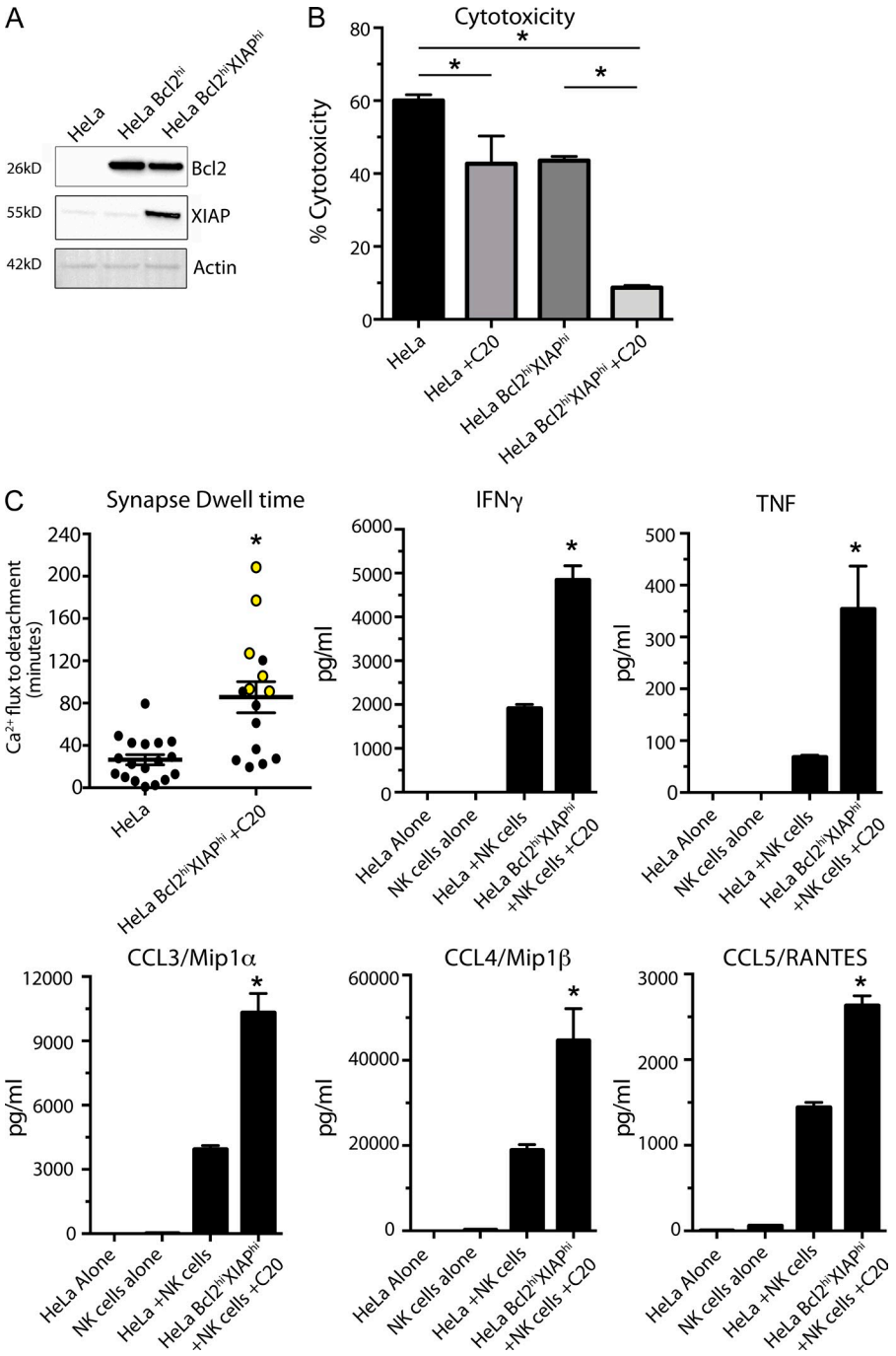

Figure 6. Blocking GzmB in target cells overexpressing Bcl-2 and XIAP causes increase in synapse dwell time and cytokine production. (A) Western blot analysis of unmodified, Bcl-2–overexpressing, or both Bcl-2– and XIAP-overexpressing HeLa cells. (B) Cytotoxicity assay of human NK cells cocultured with ^{51}Cr-labeled HeLa cells (parental or overexpressing Bcl-2 and XIAP) in the presence or absence of the human GzmB inhibitor compound 20 (C20). Shown is the percentage of specific ^{51}Cr release at E/T of 10:1 of three independent pooled experiments (mean ± SEM). Statistical significance (*, $P < 0.05$) is shown. (C) Fluo-4–AM-labeled human NK cells were added to HeLa cells or HeLa Bcl-2^{hi}XIAP^{hi} cells in the presence of C20 to inhibit GzmB during time-lapse microscopy. After conjugate formation, synapse time was measured from the first Ca^{2+} flux in NK cell until it detached from the target cell and is shown as synapse dwell time (mean minutes ± SEM; $n = 18$ and 15, respectively). Each data point represents one conjugate; data points filled with yellow indicate conjugates, where NK cells were still attached to the targets at the end of the video, underrepresenting the attachment time. The supernatant from these experiments were then analyzed for cytokine secretion by CBA, and shown is the concentration of cytokines produced after 5 h (mean pg/ml ± SD of representative experiment of two). Statistical significance was determined by Tukey's post-hoc ANOVA. *, $P < 0.05$.

via bystander activation, which then undergo dysregulated clonal expansion owing to the absence of Prf (Tough and Sprent, 1998; Badovinac et al., 2000). Thus, in the absence of Prf, a localized insult becomes systemic when NK cells cannot eliminate the initiating target.

A far greater surprise is our finding that delaying target cell death by a killer cell that secretes normal amounts of Prf/GzmAB has a very similar outcome; indeed, caspase blockade in the target cell virtually phenocopied Prf (or GzmAB) deficiency in the killer cell with respect to prolonged synapse duration, repetitive calcium signaling, cytokine hypersecretion, and macrophage activation. It is extremely common for virus-infected or transformed cells to have defects of their apoptotic machinery because of the specific gene products encoded by viruses to counteract the immune response and delay cell death or the genetic instability inherent in cancer cells, respectively. If our proposed mechanism is correct, it provides a ready explanation for the far more common secondary hemophagocytic syndromes that occur in infectious and autoimmune diseases and in some cancers (particularly

hematopoietic cancers), both in children and adults. Our findings may also have significant implications for understanding the anticancer immune response. Resistance to apoptosis is a hallmark of human cancers and can commonly occur through overexpression of antiapoptotic molecules such as Bcl-2 or IAP (Tsujimoto et al., 1984) or deletions in proapoptotic pathways (Fulda, 2009). In principle, an antigenic tumor cell that is resistant to apoptosis may delay CTL detachment, resulting both in the death of fewer tumor cells and skewing of the inflammatory response. Enhanced proinflammatory cytokine production may in turn influence the immune infiltrate in a tumor, including the content and state of activation of tumor-infiltrating macrophages.

The current study resolves a key question in immunopathology, namely the relationship between the failure to kill target cells through the Prf pathway and inflammation. It also supports the importance of understanding the mechanism of IS breakage and cytotoxic lymphocyte detachment from target cells, an essential factor responsible for their serial killing capacity. This work provides a molecular and cellular basis for the immune dysregulation observed in FHL patients and is likely to have wider implications for understanding and shaping tumor immunity and immunotherapy.

MATERIALS AND METHODS

Cell culture. MC57 (mouse fibrosarcoma) and human HeLa cells were maintained in DMEM (Invitrogen) supplemented with 10% (vol/vol) heat-inactivated FCS and 2 mM L-glutamine. HeLa cells expressing cytochrome *c*–GFP (referred to as HeLa in this manuscript) or also expressing Bcl-2 and/or XIAP are previously described (Waterhouse et al., 2006; Sedelies et al., 2008) and were a gift from N. Waterhouse (QIMR Berghofer Medical Research Institute, Brisbane, Queensland, Australia). Human Boleth (HLA-A2) target cells were grown in RPMI 1640 with 5% heat-inactivated human serum, 2 mM L-glutamine, and 100 µM nonessential amino acids.

Animals. 6–8-wk-old female C57BL/6.OTI and OTI lacking either Prf1 or GzmAB were kept in specific pathogen–free conditions at the Peter MacCallum Cancer Centre. Experiments respected institutional guidelines and were approved by the Peter MacCallum Cancer Centre animal ethics committee (E486).

Purification of mouse cytotoxic lymphocytes. Primary CTLs were isolated from the spleens of C57BL/6.OTI, OTI.GzmAB$^{-/-}$, or OTI.Prf$^{-/-}$ mice and activated with OVA_{257} peptide, as described previously (Jenkins et al., 2009). Cells were Ficoll purified on day 4 and used on day 6 or 7. Mouse NK cells were isolated from spleens by negative selection using the MACS NK isolation kit and autoMACS separator (Miltenyi Biotec). Isolated NK cells were maintained at 7×10^5 cells/ml in RPMI 1640 medium containing 1000 U/ml human IL-2 for 6–8 d before use.

Generation of mouse macrophages. Bone marrow was collected from OTI mice in PBS, and red blood cells were lysed and then resuspended at 10^6 in media containing m-CSF (BioLengend) at 50 ng/ml. Cells were cultured for 5 d before using in assays.

Generation of influenza-specific human CTLs. Human influenza matrix peptide–specific CTL clones were generated as described previously (Campbell et al., 2008). In brief, PBMCs from an HLA A0201–positive donor were cultured with influenza matrix peptide 58–66 (GILGFVFTL) at 1 µM (supplied by GL-Biochem) for 3 d in RPMI 1640 supplemented with 5% (vol/vol) pooled human serum. After 3 d, 20 U/ml IL-2 and 5 ng/ml IL-5 (PeproTech) were added, and the cells were cultured for a further 7 d. IFN-γ–secreting $CD8^+$ cells were detected after restimulation with peptide and irradiated PBMCs by surface-capture staining (Miltenyi Biotec), and single clones were generated (Mannering et al., 2005). CTLs were maintained in RPMI 1640, 5% (vol/vol) human serum, 2 mM L-glutamine, 100 µM nonessential amino acids, and 100 U/ml rIL-2.

Purification of human NK cells. NK cells were isolated from human peripheral blood by negative selection using the MACS NK isolation kit. NK cell ($CD3^-CD56^+$) content was assessed by flow cytometry and was >95% for all experiments. NK cells were maintained at 10^6 cells/ml in RPMI 1640 NK medium (10% [vol/vol] heat-inactivated FCS, 2 mM L-glutamine, 10 mM Hepes, 1 mM sodium pyruvate, 100 µM nonessential amino acids, and 50 µM 2-ME) containing 25 U/ml human rIL-2 for 24–48 h before use.

Live cell confocal microscopy. Live cell microscopy was performed as described previously (Lopez et al., 2013a). Target cells were prepared for live cell imaging by seeding 3×10^4 MC57 cells into each well of an 8-well chamber slide (ibidi) and incubating overnight at 37°C/10% CO_2. For $CD8^+$ T cell experiments, MC57 and Prf$^{-/-}$ CTLs or Boleth target cells were pulsed for 1 h with 1 µM OVA_{257} or flu_{58-86} peptide, respectively. Suspension target cells were adhered to chamber slides 15 min before imaging by incubating in serum-free media at 37°C. 2×10^4 fluo-4–labeled (labeled for 20 min with 1 µM fluo-4 and 0.02% [wt/vol] Pluronic F-127 carrier at 37°C/10% CO_2) NK cells or CTLs were added to 8-well chamber slides containing adherent targets in media containing 100 µM PI. Chamber slides were mounted on a heated stage within a temperature-controlled chamber maintained at 37°C and constant CO_2 concentrations (5%) and infused using a gas incubation system with active gas mixer (The Brick; ibidi). Optical sections were acquired through the center of the cells by sequential scans of fluo-4 (excitation 488 nm) and PI (excitation 561 nm) or brightfield/differential interference contrast on a TCS SP5 confocal microscope (Leica) using a 40× (NA 0.85) air objective and LAS AF software (Leica). For the 488 and 561 channels, the pinhole was set to 4.2 AU, giving a section thickness of 5 µM and XY pixel size of 378.8 nM. Images were acquired at ∼6–7 frames/min. Some experiments were performed in the presence of 40 µM QVD (Merck). Image analysis was performed using LAS AF Lite software (Leica) or MetaMorph Imaging Series 7 software (Universal Imaging). Statistical analyses used Prism 5 software (GraphPad Software) and ANOVA Tukey's test.

Cytokine bead array (CBA) assays. Cytokine was measured from 10 µl of culture supernatant of effector lymphocytes and target cells (with or without peptide) at a 5:1 E/T ratio, using CBA Flex sets (BD), for mouse or human IFN-γ, TNF, IL-2, IL-6, IL-1α, IL-1β, Mip1α (CCL3), Mip1β (CCL4), and RANTES (CCL5) according to the manufacturer's instructions. Samples were analyzed on a FACS VERSE using FCAP Array software version 3.0 (BD).

Immunodepletion of CCL3. Effector OTI CTLs were mixed with MC57-OVA_{257} targets at 5:1 E/T ratio for 5 h, and then supernatant was incubated with 2 µg anti-CCL3 antibody for 3 h at 4°C, before adding Protein A and incubating overnight at 4°C. The supernatant was collected and 200 µl added to 10^5 syngeneic macrophages per well in a 96-well plate and incubated at 37°C, 5% CO_2 for 48 h. Medium was collected from the macrophage culture, and a CBA was performed examining for CCL3, IL-6, and TNF (control) production.

Statistical analysis. Statistical analyses were performed using Prism 6 software (GraphPad Software). Asterisks refer to $P < 0.05$. Statistical tests applied are listed in the figure legends.

Ethics. Experiments involving human primary cells were approved by the Peter MacCallum Cancer Centre Human Research Ethics Committee (approval number 12/73) and St Vincent's Hospital Human Research Ethics Committee (approval number 135/08).

Flow cytometry. Antibodies used to examine the surface expression of proteins by flow cytometry were anti-CD11b–APC-Cy7, anti–F4/80-FITC, and anti–MHCI-PE (BD). Cells were incubated with antibodies for 30 min on ice and then washed and analyzed using a FACSCanto II analyzer (BD).

Cytotoxicity assay. Cytotoxicity was examined by labeling target cells with 100 µCi ^{51}Cr for 90 min at 37°C before washing and adding effector cells serially diluted at various E/T ratios. Cells were incubated for various times, and then the percentage of target cell lysis was calculated as 100 × (^{51}Cr release from targets with effectors − ^{51}Cr release from targets alone)/(^{51}Cr release from targets with 1% Triton X-100 − ^{51}Cr release from targets alone). The level of ^{51}Cr release from targets alone did not exceed 10% of the total ^{51}Cr release from targets with 1% Triton X-100.

Online supplemental material. Fig. S1 shows a killing assay in cells lacking effector molecules. Fig. S2 shows flow cytometry of bone marrow–derived macrophages. Video 1 shows live cell imaging of mouse OTI T cells killing a cancer target and rapidly detaching. Video 2 shows live cell imaging of a mouse OTI.Prf$^{-/-}$ in long synapse with a cancer target. Video 3 shows live cell imaging of a mouse OTI.GzmAB$^{-/-}$ in long synapse with a cancer target. Video 4 shows live cell imaging of a mouse OTI killing an MC57 cancer target. Video 5 shows a human CD8$^+$ T cell rapidly killing a cancer target. Video 6 shows a human CD8$^+$ T cell displaying delayed death of target in the presence of caspase inhibitor. Online supplemental material is available at http://www.jem.org/cgi/content/full/jem.20140964/DC1.

We thank Nigel Waterhouse for supply of reagents; Jill Danne, Sarah Ellis, and Chad Johnson for assistance with microscopy; and Ralph Rossi, Viki Milovac, and Sophie Curcio for assistance with flow cytometry.

M.R. Jenkins is supported by a National Health and Medical Research Council of Australia (NHMRC)/R.G. Menzies postdoctoral training fellowship and an NHMRC New Investigator Project Grant. J.A. Lopez is supported by an NHMRC postdoctoral training fellowship. D.M. Andrews is supported by an NHMRC Career Development Fellowship. I. Voskoboinik and J.A. Trapani are supported by fellowships and project and program grants from the NHMRC. S.I. Mannering is supported by the NHMRC, JDRF, and Diabetes Australia Research Trust (DART).

The authors declare no competing financial interests.

Submitted: 21 May 2014
Accepted: 30 January 2015

REFERENCES

Badovinac, V.P., A.R. Tvinnereim, and J.T. Harty. 2000. Regulation of antigen-specific CD8$^+$ T cell homeostasis by perforin and interferon-γ. *Science*. 290:1354–1357. http://dx.doi.org/10.1126/science.290.5495.1354

Campbell, P.D., E. Estella, N.L. Dudek, G. Jhala, H.E. Thomas, T.W. Kay, and S.I. Mannering. 2008. Cytotoxic T-lymphocyte–mediated killing of human pancreatic islet cells in vitro. *Hum. Immunol.* 69:543–551. http://dx.doi.org/10.1016/j.humimm.2008.06.008

Caserta, T.M., A.N. Smith, A.D. Gultice, M.A. Reedy, and T.L. Brown. 2003. Q-VD-OPh, a broad spectrum caspase inhibitor with potent anti-apoptotic properties. *Apoptosis*. 8:345–352. http://dx.doi.org/10.1023/A:1024116916932

Choi, P.J., and T.J. Mitchison. 2013. Imaging burst kinetics and spatial coordination during serial killing by single natural killer cells. *Proc. Natl. Acad. Sci. USA*. 110:6488–6493. http://dx.doi.org/10.1073/pnas.1221312110

Deveraux, Q.L., and J.C. Reed. 1999. IAP family proteins—suppressors of apoptosis. *Genes Dev.* 13:239–252. http://dx.doi.org/10.1101/gad.13.3.239

Ferlazzo, G. 2012. In vivo evidence for dendritic cell lysis by NK cells: Hints on improving cancer vaccines by targeting NK cell activation. *OncoImmunology*. 1:1635–1636. http://dx.doi.org/10.4161/onci.21682

Ferlazzo, G., M.L. Tsang, L. Moretta, G. Melioli, R.M. Steinman, and C. Münz. 2002. Human dendritic cells activate resting natural killer (NK) cells and are recognized via the NKp30 receptor by activated NK cells. *J. Exp. Med.* 195:343–351. http://dx.doi.org/10.1084/jem.20011149

Fulda, S. 2009. Tumor resistance to apoptosis. *Int. J. Cancer*. 124:511–515. http://dx.doi.org/10.1002/ijc.24064

Gerosa, F., B. Baldani-Guerra, C. Nisii, V. Marchesini, G. Carra, and G.Trinchieri. 2002. Reciprocal activating interaction between natural killer cells and dendritic cells. *J. Exp. Med.* 195:327–333. http://dx.doi.org/10.1084/jem.20010938

Hogquist, K.A., S.C. Jameson, W.R. Heath, J.L. Howard, M.J. Bevan, and F.R. Carbone. 1994. T cell receptor antagonist peptides induce positive selection. *Cell*. 76:17–27. http://dx.doi.org/10.1016/0092-8674(94)90169-4

Hoves, S., V.R. Sutton, N.M. Haynes, E.D. Hawkins, D. Fernández Ruiz, N. Baschuk, K.A. Sedelies, M. Schnurr, J. Stagg, D.M. Andrews, et al. 2011. A critical role for granzymes in antigen cross-presentation through regulating phagocytosis of killed tumor cells. *J. Immunol.* 187:1166–1175. http://dx.doi.org/10.4049/jimmunol.1001670

Janka, G.E. 2012. Familial and acquired hemophagocytic lymphohistiocytosis. *Annu. Rev. Med.* 63:233–246. http://dx.doi.org/10.1146/annurev-med-041610-134208

Jenkins, M.R., and G.M. Griffiths. 2010. The synapse and cytolytic machinery of cytotoxic T cells. *Curr. Opin. Immunol.* 22:308–313. http://dx.doi.org/10.1016/j.coi.2010.02.008

Jenkins, M.R., K. Kedzierska, P.C. Doherty, and S.J. Turner. 2007. Heterogeneity of effector phenotype for acute phase and memory influenza A virus-specific CTL. *J. Immunol.* 179:64–70. http://dx.doi.org/10.4049/jimmunol.179.1.64

Jenkins, M.R., J. Mintern, N.L. La Gruta, K. Kedzierska, P.C. Doherty, and S.J. Turner. 2008. Cell cycle-related acquisition of cytotoxic mediators defines the progressive differentiation to effector status for virus-specific CD8$^+$ T cells. *J. Immunol.* 181:3818–3822. http://dx.doi.org/10.4049/jimmunol.181.6.3818

Jenkins, M.R., A. Tsun, J.C. Stinchcombe, and G.M. Griffiths. 2009. The strength of T cell receptor signal controls the polarization of cytotoxic machinery to the immunological synapse. *Immunity*. 31:621–631. http://dx.doi.org/10.1016/j.immuni.2009.08.024

Jordan, M.B., D. Hildeman, J. Kappler, and P. Marrack. 2004. An animal model of hemophagocytic lymphohistiocytosis (HLH): CD8$^+$ T cells and interferon gamma are essential for the disorder. *Blood*. 104:735–743. http://dx.doi.org/10.1182/blood-2003-10-3413

Kägi, D., B. Ledermann, K. Bürki, P. Seiler, B. Odermatt, K.J. Olsen, E.R. Podack, R.M. Zinkernagel, and H. Hengartner. 1994. Cytotoxicity mediated by T cells and natural killer cells is greatly impaired in perforin-deficient mice. *Nature*. 369:31–37. http://dx.doi.org/10.1038/369031a0

Kuželová, K., D. Grebeňová, and B. Brodská. 2011. Dose-dependent effects of the caspase inhibitor Q-VD-OPh on different apoptosis-related processes. *J. Cell. Biochem.* 112:3334–3342. http://dx.doi.org/10.1002/jcb.23263

La Gruta, N.L., P.C. Doherty, and S.J. Turner. 2006. A correlation between function and selected measures of T cell avidity in influenza virus-specific CD8$^+$ T cell responses. *Eur. J. Immunol.* 36:2951–2959. http://dx.doi.org/10.1002/eji.200636390

Lopez, J.A., M.R. Jenkins, J.A. Rudd-Schmidt, A.J. Brennan, J.C. Danne, S.I. Mannering, J.A. Trapani, and I. Voskoboinik. 2013a. Rapid and unidirectional perforin pore delivery at the cytotoxic immune synapse. *J. Immunol.* 191:2328–2334. http://dx.doi.org/10.4049/jimmunol.1301205

Lopez, J.A., O. Susanto, M.R. Jenkins, N. Lukoyanova, V.R. Sutton, R.H. Law, A. Johnston, C.H. Bird, P.I. Bird, J.C. Whisstock, et al. 2013b. Perforin forms transient pores on the target cell plasma membrane to facilitate rapid access of granzymes during killer cell attack. *Blood*. 121:2659–2668. http://dx.doi.org/10.1182/blood-2012-07-446146

Mannering, S.I., J.A. Dromey, J.S. Morris, D.J. Thearle, K.P. Jensen, and L.C. Harrison. 2005. An efficient method for cloning human autoantigen-specific T cells. *J. Immunol. Methods*. 298:83–92. http://dx.doi.org/10.1016/j.jim.2005.01.001

Pachlopnik Schmid, J., C.H. Ho, F. Chrétien, J.M. Lefebvre, G. Pivert, M. Kosco-Vilbois, W. Ferlin, F. Geissmann, A. Fischer, and G. de Saint Basile. 2009. Neutralization of IFNγ defeats haemophagocytosis in LCMV-infected perforin- and Rab27a-deficient mice. *EMBO Mol. Med.* 1:112–124. http://dx.doi.org/10.1002/emmm.200900009

Piccioli, D., S. Sbrana, E. Melandri, and N.M. Valiante. 2002. Contact-dependent stimulation and inhibition of dendritic cells by natural killer cells. *J. Exp. Med.* 195:335–341. http://dx.doi.org/10.1084/jem.20010934

Sedelies, K.A., A. Ciccone, C.J. Clarke, J. Oliaro, V.R. Sutton, F.L. Scott, J. Silke, O. Susanto, D.R. Green, R.W. Johnstone, et al. 2008. Blocking granule-mediated death by primary human NK cells requires both protection of mitochondria and inhibition of caspase activity. *Cell Death Differ.* 15:708–717. http://dx.doi.org/10.1038/sj.cdd.4402300

Sieni, E., V. Cetica, Y. Hackmann, M.L. Coniglio, M. Da Ros, B. Ciambotti, D. Pende, G. Griffiths, and M. Aricò. 2014. Familial hemophagocytic lymphohistiocytosis: when rare diseases shed light on immune system functioning. *Front. Immunol.* 5:167. http://dx.doi.org/10.3389/fimmu.2014.00167

Stepp, S.E., R. Dufourcq-Lagelouse, F. Le Deist, S. Bhawan, S. Certain, P.A. Mathew, J.I. Henter, M. Bennett, A. Fischer, G. de Saint Basile, and V. Kumar. 1999. Perforin gene defects in familial hemophagocytic lymphohistiocytosis. *Science.* 286:1957–1959. http://dx.doi.org/10.1126/science.286.5446.1957

Strasser, A., A.W. Harris, M.L. Bath, and S. Cory. 1990a. Novel primitive lymphoid tumours induced in transgenic mice by cooperation between myc and bcl-2. *Nature.* 348:331–333. http://dx.doi.org/10.1038/348331a0

Strasser, A., A.W. Harris, D.L. Vaux, E. Webb, M.L. Bath, J.M. Adams, and S. Cory. 1990b. Abnormalities of the immune system induced by dysregulated bcl-2 expression in transgenic mice. *Curr. Top. Microbiol. Immunol.* 166:175–181.

Strasser, A., S. Cory, and J.M. Adams. 2011. Deciphering the rules of programmed cell death to improve therapy of cancer and other diseases. *EMBO J.* 30:3667–3683. http://dx.doi.org/10.1038/emboj.2011.307

Susanto, O., S.E. Stewart, I. Voskoboinik, D. Brasacchio, M. Hagn, S. Ellis, S. Asquith, K.A. Sedelies, P.I. Bird, N.J. Waterhouse, and J.A. Trapani. 2013. Mouse granzyme A induces a novel death with writhing morphology that is mechanistically distinct from granzyme B-induced apoptosis. *Cell Death Differ.* 20:1183–1193. http://dx.doi.org/10.1038/cdd.2013.59

Sutton, V.R., D.L. Vaux, and J.A. Trapani. 1997. Bcl-2 prevents apoptosis induced by perforin and granzyme B, but not that mediated by whole cytotoxic lymphocytes. *J. Immunol.* 158:5783–5790.

Sutton, V.R., K. Sedelies, G. Dewson, M.E. Christensen, P.I. Bird, R.W. Johnstone, R.M. Kluck, J.A. Trapani, and N.J. Waterhouse. 2012. Granzyme B triggers a prolonged pressure to die in Bcl-2 overexpressing cells, defining a window of opportunity for effective treatment with ABT-737. *Cell Death Dis.* 3:e344. http://dx.doi.org/10.1038/cddis.2012.73

Terrell, C.E., and M.B. Jordan. 2013. Perforin deficiency impairs a critical immunoregulatory loop involving murine $CD8^+$ T cells and dendritic cells. *Blood.* 121:5184–5191. http://dx.doi.org/10.1182/blood-2013-04-495309

Tough, D.F., and J. Sprent. 1998. Bystander stimulation of T cells in vivo by cytokines. *Vet. Immunol. Immunopathol.* 63:123–129. http://dx.doi.org/10.1016/S0165-2427(98)00088-9

Tsujimoto, Y., L.R. Finger, J. Yunis, P.C. Nowell, and C.M. Croce. 1984. Cloning of the chromosome breakpoint of neoplastic B cells with the t(14;18) chromosome translocation. *Science.* 226:1097–1099. http://dx.doi.org/10.1126/science.6093263

van Dommelen, S.L., N. Sumaria, R.D. Schreiber, A.A. Scalzo, M.J. Smyth, and M.A. Degli-Esposti. 2006. Perforin and granzymes have distinct roles in defensive immunity and immunopathology. *Immunity.* 25:835–848. http://dx.doi.org/10.1016/j.immuni.2006.09.010

Voskoboinik, I., and J.A. Trapani. 2013. Perforinopathy: a spectrum of human immune disease caused by defective perforin delivery or function. *Front. Immunol.* 4:441. http://dx.doi.org/10.3389/fimmu.2013.00441

Waterhouse, N.J., K.A. Sedelies, V.R. Sutton, M.J. Pinkoski, K.Y. Thia, R. Johnstone, P.I. Bird, D.R. Green, and J.A. Trapani. 2006. Functional dissociation of $\Delta\Psi$m and cytochrome c release defines the contribution of mitochondria upstream of caspase activation during granzyme B-induced apoptosis. *Cell Death Differ.* 13:607–618. http://dx.doi.org/10.1038/sj.cdd.4401772

Willoughby, C.A., H.G. Bull, M. Garcia-Calvo, J. Jiang, K.T. Chapman, and N.A. Thornberry. 2002. Discovery of potent, selective human granzyme B inhibitors that inhibit CTL mediated apoptosis. *Bioorg. Med. Chem. Lett.* 12:2197–2200. http://dx.doi.org/10.1016/S0960-894X(02)00363-3

Yeretssian, G., K. Doiron, W. Shao, B.R. Leavitt, M.R. Hayden, D.W. Nicholson, and M. Saleh. 2009. Gender differences in expression of the human caspase-12 long variant determines susceptibility to *Listeria monocytogenes* infection. *Proc. Natl. Acad. Sci. USA.* 106:9016–9020. http://dx.doi.org/10.1073/pnas.0813362106